22

Cardiovascular Applications

Miguel Hernandez-Pampaloni

An improved understanding of the pathophysiology of myocardial ischemia combined with the development of new diagnostic modalities has substantially modified the concepts of myocardial blood flow (MBF) and left ventricular function in coronary artery disease (CAD). Positron emission tomography (PET) has emerged as a unique tool to characterize physiologic and pathologic processes, and it already plays a significant role in different areas of clinical medicine, including cardiology. Cardiac PET is based on the properties of positron emitters and radiation detection to provide a noninvasive and in vivo assessment of regional myocardial perfusion and metabolism. Different study protocols have been largely used in the adult population to detect and grade the severity of coronary artery disease during the last two decades using cardiac PET technology. Further, cardiac PET using fluorine-18 (^{18}F) 2-fluoro-2-deoxyglucose (FDG) is considered the gold standard imaging modality for the assessment of myocardial viability (1) and is well recognized as providing accurate information on the long-term prognosis of the patients with chronic coronary ischemic disease (2).

Positron emission tomography offers unique capabilities for noninvasive assessment of regional myocardial function and can disclose information of utmost importance for the more accurate understanding of pathophysiologic processes and for the optimal management of the diseased patient. By detecting the very early functional regional abnormalities before the development of more severe structural changes, PET imaging can be useful in providing improved and preventive care to the patient. Thus, cardiac PET imaging can offer a more comprehensive understanding of the normal myocardial physiology and early recognition of functional abnormalities. This is even more important in pediatric cardiology where the early detection of myocardial dysfunction may be helpful in choosing the appropriate management for the prevention of long-term consequences. Recent surgical and technical advances in pediatric cardiology make even more important an accurate detection of potentially treatable coronary abnormalities. Positron emission tomography imaging's high spatial and

temporal resolution provides better image quality, especially important in small pediatric hearts, and it allows the quantification in absolute terms of the MBF and regional myocardial metabolism. Single photon emission computed tomography (SPECT) imaging quality is usually limited by poor resolution and the low usable activity of thallium 201 (^{201}Tl), whereas images obtained after the administration of technetium-labeled compounds are compromised by the high liver activity in close proximity to the small heart.

This chapter describes the basic principles of PET applied to the study of the heart, and presents the current and potential future clinical applications of cardiac PET in pediatric patients.

Principles of Emission Tomography Applied to the Cardiovascular System

Positron emission tomography imaging features are based on the physical properties of the positron decay. A positron has the same characteristics as an electron, except for its positive charge. Positrons are emitted from unstable nuclei (that have an excess of protons) that dispose of their excess charge by emitting a positron. At the end of the positron range, after losing its kinetic energy, a positron combines with an electron and the two particles annihilate. The annihilation coincidence detection of the two colinear 511-keV gamma rays photons, emitted in diametrically opposite directions by opposing scintillator detectors, is the essence of the PET imaging formation (3). To detect the location of the annihilation event, detectors are placed on opposite sides of the source and are connected in a coincidence detection circuit. When a given event is recorded simultaneously, positron annihilation is assumed to have taken place on the line between the detectors, and hence the location can be accurately determined.

Radiopharmaceuticals

Cardiac PET studies are performed with radiopharmaceuticals specifically synthesized to assess determined cardiac functions or biochemical processes and with radiopharmaceuticals that have applications in other disciplines. The radiolabeled positron-emitting tracers used in cardiac PET studies are produced by a cyclotron or by a generator system. Currently, different processes of the heart have been studied using different radiopharmaceuticals (Table 22.1). The radiation exposure to PET radiotracers is lower compared to other radionuclides used for nuclear cardiology studies (Table 22.2).

Evaluation of Myocardial Blood Flow

The development of suitable radiotracers and appropriate mathematical models applied to PET imaging has been shown to allow for the noninvasive and accurate quantification of regional MBF. Different radiotracers have been used for measuring MBF, including nitrogen-13–labeled ammonia ($^{13}NH_3$) (4–6), oxygen-15 (^{15}O)-labeled water (^{15}O-

Table 22.1. Principal PET tracers for cardiac imaging

Radionuclide	Radiopharmaceutical	Physical half-life	Mean positron range	Production	Cardiac application
^{13}N	Ammonia	10.0 min	0.7 mm	Cyclotron	Blood flow
^{82}Rb	Rubidium chloride	78 s	2.6 mm	Generator	Blood flow
^{15}O	Water	2.0 min	1.1 mm	Cyclotron	Blood flow, perfusable tissue index
^{18}F	Deoxyglucose	110 min	0.2 mm	Cyclotron	Glucose metabolism
^{11}C	Acetate palmitate	20 min	0.28 mm	Cyclotron	Blood flow, oxygen consumption fatty acid metabolism

H_2O) (7–9), the potassium analogue rubidium-82 (^{82}Rb) (10), copper-62 (^{62}Cu)-pyruvaldehyde bis(N4-methylthio-semicarbazone (^{62}Cu-PTSM) (11,12), gallium-68 (^{68}Ga)-labeled albumin microspheres (13), and potassium 38 (^{38}K) (14). The choice of a specific radiotracer is finally frequently determined by different factors besides their physical properties, such as an individual institution's preference, experience, or accessibility. Currently, $^{13}NH_3$, ^{15}O-H_2O, and ^{82}Rb are the most widely used PET perfusion tracers. Generator-produced ^{82}Rb has the advantages of not requiring a cyclotron and having a very short half-life (78 seconds), making it attractive for one-session rest/stress imaging. ^{82}Rb has a low first-pass myocardial extraction fraction (50% to 60%) that results in a nonlinear uptake in relation to blood flow, particularly at high flow rates (15). As a potassium analogue, ^{82}Rb is retained in the myocardium and equilibrates with the cellular potassium pool. Because of the dependence on the flow rate and the metabolic state,

Table 22.2. Dosimetry in cardiac pediatric nuclear medicine

	^{99m}Tc-sestamibi	^{201}Tl	^{13}N-ammonia	^{18}F-FDG
	Effective dose equivalent (mSv/MBq)			
Newborn (3.5 kg)	0.120	11.00	0.0320	0.310
1-yr-old (10 kg)	0.058	6.90	0.0130	0.100
5-yr-old (18 kg)	0.041	4.90	0.0067	0.077
10-yr-old (31 kg)	0.027	4.10	0.0043	0.050
15-yr-old (56 kg)	0.019	0.68	0.0028	0.038
Adult (70 kg)	0.015	0.34	0.0022	0.030
Critical organ	Kidney	Kidney	Bladder wall	Bladder wall
	Dose equivalent per body weight			
Newborn (3.5 kg)	0.89	12.22	0.34	1.64
1-yr-old (10 kg)	0.43	7.67	0.14	0.69
5-yr-old (18 kg)	0.30	5.44	0.07	0.41
10-yr-old (31 kg)	0.20	4.56	0.05	0.26
15-yr-old (56 kg)	0.14	0.76	0.03	0.20
Adult (70 kg)	0.11	0.38	0.02	0.16

Source: Modified from Radiopharmaceutical Internal Dose Information Center, Oak Ridge Associated Universities, Oak Ridge, Tennessee.

situations of hyperemia or metabolically impaired myocardium may limit the accuracy for quantifying MBF. $^{13}NH_3$ is a cyclotron-generated myocardial perfusion tracer with a high first-pass extraction fraction, a high tissue-to-blood contrast ratio within minutes following the radiotracer administration, and a relatively short half-life (9.8 minutes) that makes it also suitable for one-session studies. $^{13}NH_3$ is metabolically trapped in the myocardium based on the glutamine synthetase action. Under physiologic resting blood flow, the rate of metabolic conversion of $^{13}NH_3$ to glutamine inside the myocytes is sufficiently elevated to convert and retain a major fraction of $^{13}NH_3$ delivered to the myocardial tissue. However, in conditions of high flow, the amount of $^{13}NH_3$ delivered to the myocardial tissue exceeds the rate of conversion to glutamine, and therefore a significant amount of $^{13}NH_3$ is returned to the capillary blood and removed from the tissue. To overcome this nonlinear response to conditions of high flow rate, different kinetic modeling approaches have been developed (16,17). To minimize the limited spatial resolution of PET systems and the intrinsic motion of the heart, additional corrections have been included to account for the impact of the partial volume effect and spillover fraction (18,19).

^{15}O-H_2O has several attractive properties as a myocardial perfusion tracer including a high first-pass extraction fraction (nearly 100%), a freely diffusible uptake and washout mechanism limited only by myocardial perfusion, a much reduced accumulation of the tracer in background organs, and finally a short half-life (122 seconds) that permits repeated and sequential blood flow measurements. However, the rapid washout of ^{15}O-H_2O requires corrections to achieve a good tissue–blood contrast, necessary for an accurate MBF quantification. To correct for the high activity of ^{15}O-H_2O in the blood pool, an additional ^{15}O–carbon monoxide blood pool scanning, which binds hemoglobin in the red blood cells, was required to define regions of interest and delineate the vascular space. These correction techniques have recently been optimized by the generation of myocardial images directly from dynamic ^{15}O-H_2O scans, not requiring the ^{15}O-carbon monoxide blood pool scan (20,21).

Evaluation of Fatty Acid Metabolism and Oxygen Consumption

Cardiomyocytes metabolize various substrates as source of energy. Under fasting conditions, free fatty acids are the primary source of energy. Free fatty acids are extracted by the myocardium and, after the formation of long-chain acyl–coenzyme A (CoA), predominantly enter the mitochondria to suffer β-oxidation prior to going into the tricarboxylic acid cycle. The rate of fatty acid oxidation is controlled by the rate of transfer into the mitochondria. ^{11}C-palmitate, a 16-carbon, long-chain fatty acid, was the first PET radiotracer used to assess regional cardiac metabolism. Clearance of ^{11}C-palmitate follows a bioexponential kinetic model. The initial rapid-phase clearance reflects the immediate oxidation and the elimination of carbon dioxide. The second phase is believed to represent the incorporation of the radiotracer into

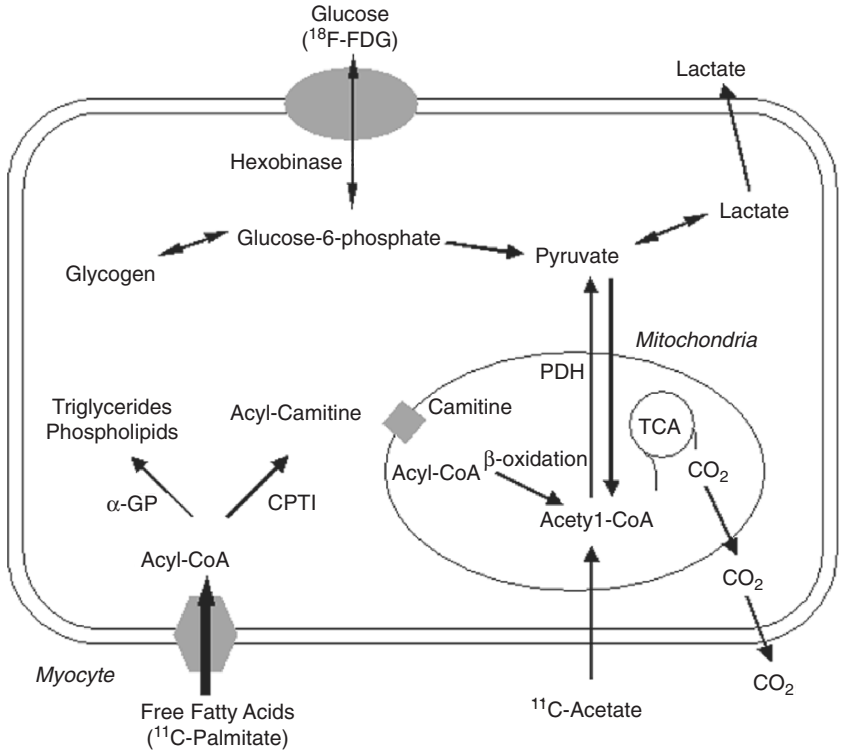

Figure 22.1. Radiotracers that can be used by PET to investigate different myocardial metabolic pathways.

the lipid metabolism as triglycerides and its final oxidation (22). The kinetics of ^{11}C-palmitate may theoretically be useful to evaluate cardiac metabolism in situations of ischemic compromise. During ischemia, the rate of elimination of ^{11}C-palmitate is decreased with a reduced oxidation of fatty acids. On the other hand, the increased cardiac work would produce an accelerated clearance of the radiotracer as the oxidative metabolism would be increased. However, the main disadvantage of this compound is the complexity of its kinetics because a very rapid clearance from the blood pool and β-oxidation allows only a very short time of analysis (Fig. 22.1).

To overcome the limitations presented by ^{11}C-palmitate, ^{11}C-acetate has been proposed as an alternative to evaluate oxidative cardiac metabolism (23,24). ^{11}C-palmitate is extracted proportionally to MBF with a first-pass extraction fraction of approximately 50% under resting conditions. Once inside the myocyte, ^{11}C-palmitate is converted to ^{11}C-acetyl-CoA, which enters the tricarboxylic acid cycle in the mitochondria (21,22). Clearance of ^{11}C activity in the form of ^{11}C-CO_2 does not occur for 4 to 5 minutes after tracer delivery, reflecting MBF except in conditions of high oxygen demand. Kinetics of ^{11}C-palmitate has allowed the quantification of oxygen consumption from the myocardial clearance rate as a parameter of the oxidative metabolism and MBF

and its correlation with the presence of ischemia when this oxygen consumption diminishes (25–27).

Evaluation of Glucose Metabolism

In contrast to fasting conditions where free fatty acids predominate as a source of myocardial energy, after an ingestion of carbohydrates plasma glucose and insulin levels increase and levels of free fatty acids decline. In response, oxidation of free fatty acids decreases and utilization and oxidation of glucose increases. When myocardial ischemia ensues, contractile function declines, oxidation of free fatty acids decreases, and uptake and metabolism of glucose increase. Then glucose transport and metabolism are upregulated during ischemic conditions and after the complete resolution of these episodes, most likely due to an upregulation of the glucose transporter GLUT-1 (28,29). Regional cardiac glucose metabolic activity can be assessed with ^{18}F-FDG. The positron emitter ^{18}F (with a half-life of 109 minutes) linked to the glucose analogue FDG, passes the cellular membrane through facilitated diffusion, mostly mediated by the insulin-sensitive protein carrier GLUT-4 (30). Inside the myocyte the radiotracer is subjected to the first step of glycolysis by a hexokinase-mediated phosphorylation to FDG-6-phosphate. The phosphorylated glucose analogue becomes metabolically trapped in the myocardium so that the regional tracer activity concentrations reflect regional rates of exogenous glucose utilization. A more favorable standardized assessment of myocardial glucose utilization has been achieved assuming the conditions would have remained the same under physiologic and pathophysiologic conditions, by applying the so-called lumped constant, which corrects for the different kinetics affinities between ^{18}F-FDG and glucose itself (31).

Noninvasive approaches that assess exogenous glucose utilization, therefore, play an important role in the evaluation of myocardial viability in patients with coronary ischemic disease and left ventricular dysfunction. Because dysfunctional myocardium that can recover function after revascularization must retain sufficient blood flow and metabolic activity to sustain myocytes, the combined assessment of regional MBF and glucose metabolism provides additional and invaluable information.

Interpretation of PET Data

The acquisition of cardiac PET data can be achieved in either the static or dynamic mode. For static acquisitions prior to imaging, time is allowed after the injection of the radiotracer for adequate clearance from the bloodstream and uptake from the myocardium to obtain adequate myocardial-to-background activity ratios. Static imaging depicts the relative distribution of the radiotracers in the myocardium and is used for a semiquantitative or qualitative analysis of the distribution of the radiotracers within different regions of the myocardium. This approach, however, does not allow accurate quantifying functional myocardial processes. Imaging cardiac PET data are routinely

acquired in transaxial slices with a field of view of approximately 10 to 15 cm. Reconstruction of the attenuation-corrected projection data is usually performed by filtered backprojection. Specific software is used to realign the image information perpendicular to the long axis of the left ventricle. This allows the visualization of the radiotracer distribution along the short and long axes of the left ventricle. The interpretation of the images is based on the visualization of the short, vertical, and horizontal long axes based on the relative regional distribution of the tracer (32). Further, the evaluation of circumferential profile analysis provides a more objective way to measure regional tracer differences and is based on specific analysis software packages, similar to that introduced for SPECT analysis (5,6). For the objective assessment of myocardial perfusion defects, individual patient data are compared with a database of normal controls. The assessment of regional myocardial defects is expressed as a percentage of pixels below two standard deviations of the control population for the corresponding area of myocardium.

Detailed knowledge of the myocardial biochemical processes is required to accurately analyze different patterns of the uptake of myocardial blood flow (^{13}N-ammonia, ^{15}O-H_2O, ^{82}Rb) and myocardial metabolism radiotracers (^{18}F-FDG). Three patterns of blood flow–metabolism uptake have been described in adults and largely used to analyze severe dysfunctional myocardium for assessing the presence of recoverable and, hence, viable myocardium (4). A normal distribution of the flow radiotracer regardless of the uptake of ^{18}F-FDG is seen in normal myocardium. On the other hand, absent or severely reduced regional blood flow and glucose metabolism is observed in akinetic and dyskinetic myocardium and represents myocardial necrosis. This pattern is described as a "match defect." Finally, the maintained reduced blood flow to the myocardium produces an adaptation with a normal or slightly reduced uptake of ^{18}F-FDG. This reduced or absent MBF with normal or slightly reduced glucose metabolism within the myocytes indicates myocardial hibernation and therefore viability. This pattern, described as a "mismatch pattern," characterizes severe dysfunctional myocardium supplied by a stenotic or almost totally occluded coronary artery (Fig. 22.2). The restoration of blood flow to these myocardial regions results in recovery of contractile function and normalization of the glucose metabolism (33,34). This more probably occurs after a period of time, described as stunned myocardium, where glucose metabolism may remain elevated with a normalized blood flow and a not entirely recovered contractile function.

Positron emission tomography cardiac radiotracers and physical properties of the PET system enable the absolute quantification of myocardial biochemical processes, such as myocardial blood flow and glucose metabolism. This is based on the short half-life and high energy of the radiotracers and the high temporal and spatial resolution of the current PET systems that provides the ground to accurately measure rapid changes in tissue tracer concentrations. Quantification of myocardial processes requires dynamic acquisition and the application of

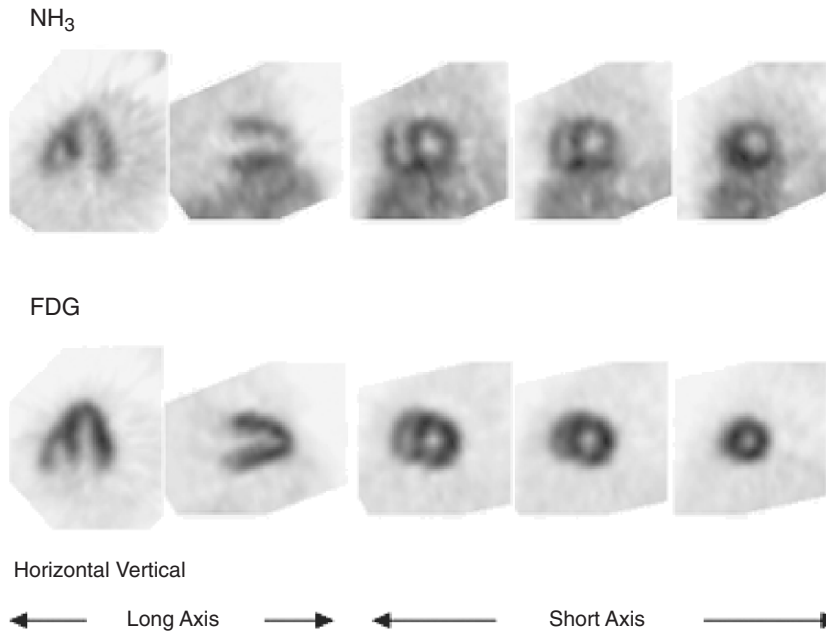

Figure 22.2. Reoriented images of the myocardial ^{13}N-ammonia (upper panel) and ^{18}F-FDG uptake (lower panel) in a patient with transposition of the great arteries after the arterial switch operation. Note the impaired perfusion in the anterolateral wall (arrows), evidenced by the decreased uptake of ^{13}N-ammonia, whereas the myocyte metabolism of ^{18}F-FDG is preserved, indicating viable myocardium. (Courtesy of Dr. Heinrich Schelbert, David Geffen School of Medicine, Los Angeles.)

tracer kinetic models (5,35). This means that the images are acquired by the system from the time of the tracer injection through a point of steady-state flux. Sampling with high temporal resolution is required to define the changes in radioactivity in the blood and the myocardial region of interest. The rapid sequential sampling and imaging enables the determination of the tracer delivery via the arterial plasma to the region of interest to define the arterial input function and the consequent tissue response to this input function. Arterial input function is generally defined by regions of interest placed over the left atrium or left ventricle to obtain temporal changes in radioactivity concentration in the different heart chambers. The rapid dynamic acquisition along with a late time frame enables the derivation of a myocardial tissue time-activity curve (19).

Dynamic acquisition, with its high volume of data, requires specific interactive software for image reconstruction, quantitative analysis, and visual presentation. The obtained regional MBF is expressed in milliliters per minute per 100 g of tissue, glucose utilization in micromoles per minute per gram of tissue, oxygen consumption in micromoles per minute per 100 g of tissue, and coronary flow reserve as the ratio of stress and resting myocardial perfusion.

Cardiac PET Protocols

Positron emission tomography studies in the pediatric population require special considerations for patient preparation and the data acquisition process. Experience in performing pediatric studies and expertise in dealing with pediatric patients will optimize the outcome of the entire study procedure minimizing the discomfort to the patients. A cardiac PET study requires the patient to remain still for the entire duration of the study. A routine myocardial blood flow–metabolism study may last up to 2 hours, and a rest/stress myocardial perfusion study may last up to 90 minutes. Thus, unlike adults, most pediatric patients would require sedation before the study is performed. This is especially necessary for infants and young children. Several intravenous premedication protocols have been used, mostly including chloral hydrate or midazolam (36,37). Due to the length of the study, further intravenous sedation may be necessary. Baseline vital signs (electrocardiogram, blood pressure, and heart rate) along with transcutaneous pulse oximetry should be recorded and monitored throughout the study.

Myocardial perfusion imaging and coronary reserve studies consist of a resting and stress examination using either pharmacologic stress (dipyridamole or adenosine) or exercise (ergometric bicycle). Patients should refrain from eating or drinking anything except water for 4 hours before the procedure, and they should abstain from caffeine-containing drinks or medications containing theophylline for 8 hours before. Adolescents should avoid cigarettes for at least 8 hours as well. Studies involving metabolic imaging with ^{18}F-FDG require a standardization of the substrate availability that optimizes myocardial glucose uptake. Older children and adolescents are routinely fasted overnight, and an oral glucose load dose is given 1 hour prior to the ^{18}F-FDG injection to facilitate glucose uptake in the myocardium. It is important to ascertain any history of diabetes or intolerance to glucose to ensure that proper steps are taken to optimize myocardial glucose uptake. Blood glucose monitoring during the study should be performed routinely to ensure that metabolic conditions are maintained along the entire acquisition process.

Clinical Applications

Coronary abnormalities, with impairments of regional myocardial perfusion, are a relevant cause of morbidity and mortality in the pediatric population. Although the experience of cardiovascular PET in pediatrics remains somewhat limited, this technique has been applied in several congenital and acquired heart diseases, providing new insights into the diseased pediatric heart and optimizing the clinical management of these patients. Recent surgical and technical advances have provided better treatment and long-term prognosis for many complex pediatric heart diseases, making the accurate diagnosis of ischemic but potentially recoverable myocardium even more important.

Transposition of the Great Arteries

In infants with transposition of the great arteries (TGA), correct cardiac anatomy is surgically restored by the arterial switch operation (ASO) of aorta and pulmonary artery. As the coronary arteries need to be excised and reinserted in the neo-aorta during the procedure, the long-term success of this operation is based on the continued patency and adequate functioning of the coronary arteries. The findings that post-surgical coronary occlusions have been described angiographically (38) and that acute myocardial infarctions and sudden deaths have been reported (39) in up to 10% of this patient population emphasize the prognostic implications of this issue. Regional reversible perfusion abnormalities were initially described by using exercise technetium-99m-sestamibi SPECT in patients following ASO (40). In contrast to SPECT imaging, higher spatial resolution of PET systems have allowed for the absolute quantification of MBF. Bengel et al. (41) were the first to report regional perfusion abnormalities with adenosine ^{13}N-ammonia PET in patients with no ischemic symptoms late after the ASO, with no correlation with any echocardiographic contractile dysfunction. They found a lower incidence of reversible perfusion defects when compared to the previous SPECT imaging studies, but quantitative hyperemic MBF and coronary flow reserve in response to adenosine were significantly lower in the patients after ASO, when compared to young healthy individuals. Similar results were described by others, which suggests that the global impairment of maximal MBF may represent alterations in the myocardial normal vasoreactivity as the early manifestation of changes in the coronary microcirculation (42). However, the procedure of coronary reimplantation alone seems to be not the only factor responsible for the myocardial perfusion abnormalities. By comparing two groups of patients with transposition of the great arteries, one after the ASO and the second after the Ross procedure to treat aortic valve disease with ^{13}N-ammonia adenosine PET, Hauser et al. (43) reported that in contrast to the patients who underwent the Ross operation, stress-induced perfusion defects and a diminished coronary flow reserve were documented in the patients after the ASO. Further follow-up and more extensive investigations are necessary to fully understand the etiology of these findings and to determine whether the reported myocardial perfusion abnormalities have significant long-term prognostic implications in these patients.

Metabolic ^{18}F-FDG imaging, along with myocardial perfusion assessment can provide useful information to identify viable but dysfunctional myocardium in patients who develop an acute cardiac event after the ASO or as a result of other coronary abnormalities. Rickers et al. (44) stated that ^{18}F-FDG–gated PET demonstrated viable myocardium in akinetic or hypokinetic regions subtended by stenotic coronary arteries after the ASO. Based on their findings, they treated patients surgically with coronary revascularization if viable myocardium was identified, whereas the patients with impaired glucose uptake, indicating myocardial scarring, were treated medically. To establish the accuracy of metabolic and perfusion PET imaging in

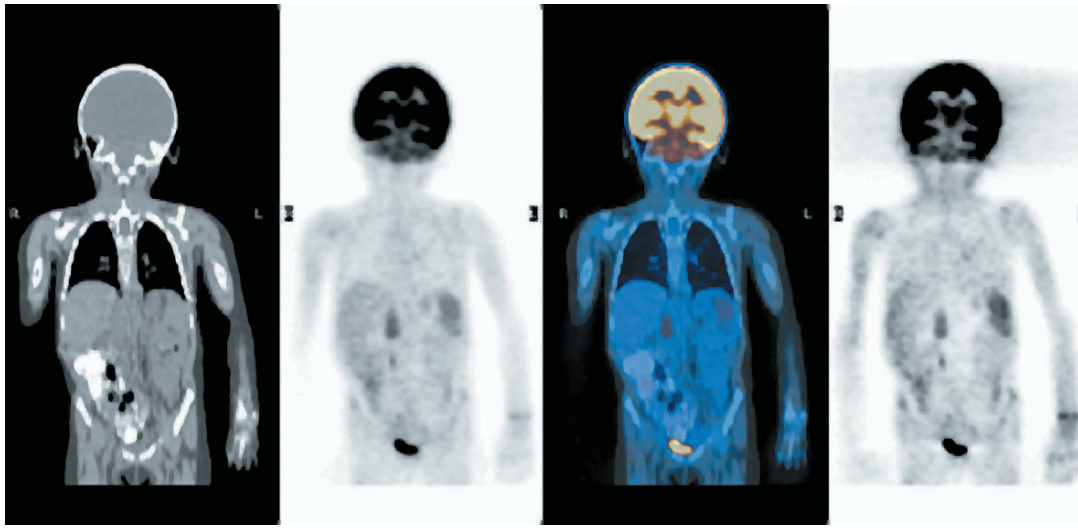

Figure 13.3. Positron emission tomography–computed tomography (PET-CT) coronal images of a 4-year-old girl with refractory neuroblastoma following bone marrow transplantation. A: CT scan. B: FDG-PET scan with attenuation correction. C: Fusion image of CT scan and FDG-PET scan with attenuation correction. D: FDG-PET scan without attenuation correction. Abnormal uptake of FDG in the abdomen is seen to the right of the midline medial to the liver, representing residual neuroblastoma.

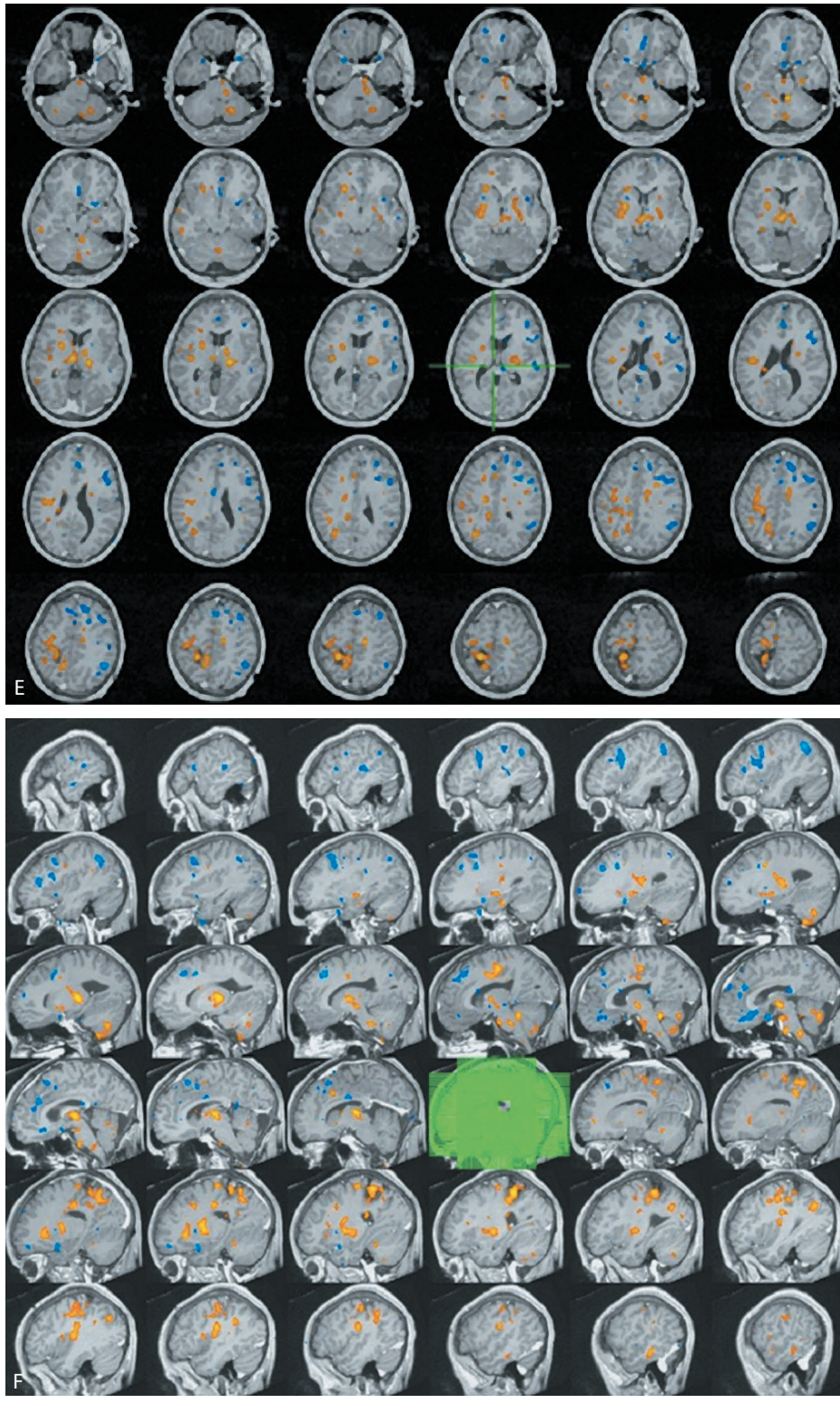

Figure 20.6. E: Statistical pixel analysis map in transverse section of significant ictal rCBF greater than interictal rCBF (yellow) or less that interictal rCBF (blue). Map shows significant ictal associated hyperemia in the region of the angioma. F: Statistical pixel analysis map in sagittal section of significant ictal rCBF greater than interictal rCBF (yellow) or less that interictal rCBF (blue). Map shows significant ictal associate hyperemia anterior to the angioma.

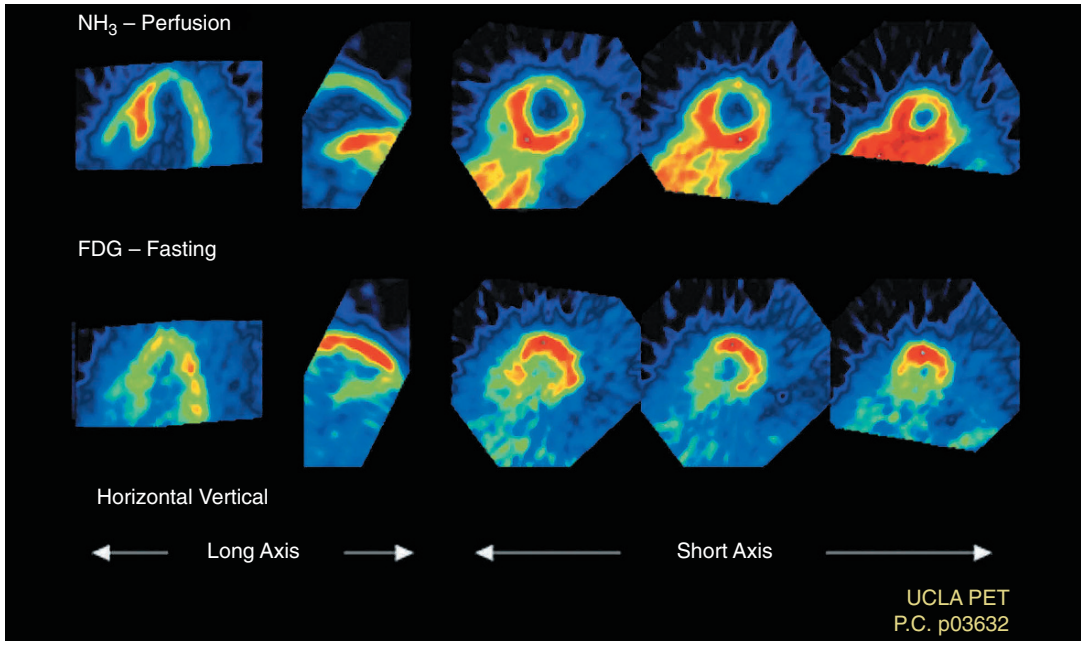

Figure 22.3. Reoriented images of the myocardial ^{13}N-ammonia (upper panel) and fasting ^{18}F-FDG uptake (lower panel) in a patient with transposition of the great arteries who had an acute episode of chest pain late after the arterial switch operation. Note the impaired perfusion in the anterolateral wall evidenced by the decreased uptake of ^{13}N-ammonia, whereas the myocyte metabolism of ^{18}F-FDG is preserved, indicating viable myocardium in that myocardial regions. (Courtesy of Dr. Heinrich Schelbert, David Geffen School of Medicine, Los Angeles.)

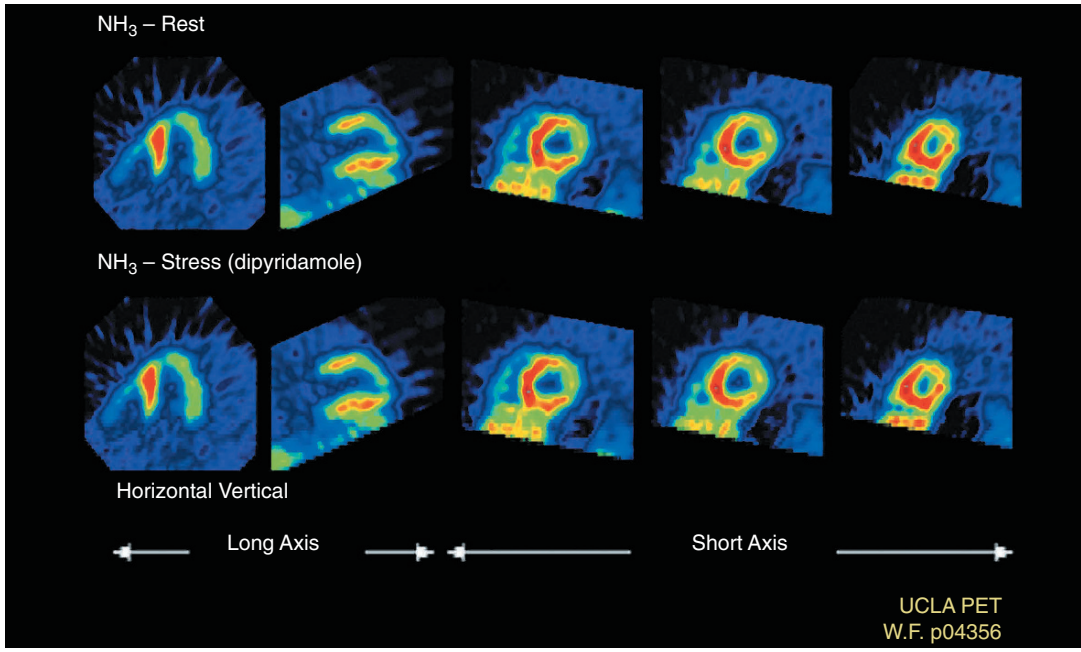

Figure 22.4. Reoriented images of the myocardial resting ^{13}N-ammonia (upper panel) and after dipyridamole-induced stress ^{13}N-ammonia (lower panel) PET study in a patient with anomalous origin of the left coronary artery arising from the pulmonary artery (ALCAPA). Note the fixed defect in the anterolateral wall that corresponds to an acute myocardial infarction in that region. (Courtesy of Dr. Heinrich Schelbert, David Geffen School of Medicine, Los Angeles.)

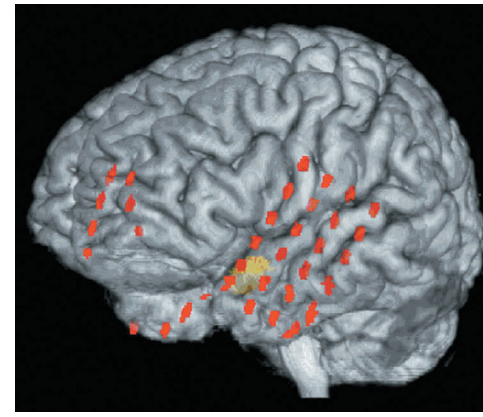

Figure 27.2. Three-dimensional (3D) reconstruction of a registered image data set. The cortical surface was rendered from MRI and red dots represent subdural EEG electrodes that were imaged with CT. The functional epileptogenic focus (orange) was defined by interictal fluorodeoxyglucose (FDG)-PET and ictal ECD–single photon emission computed tomography (SPECT).

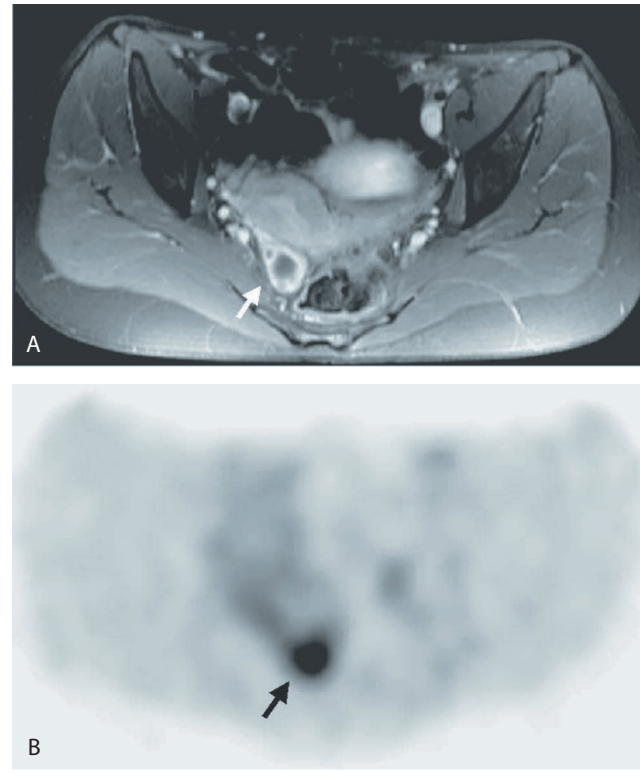

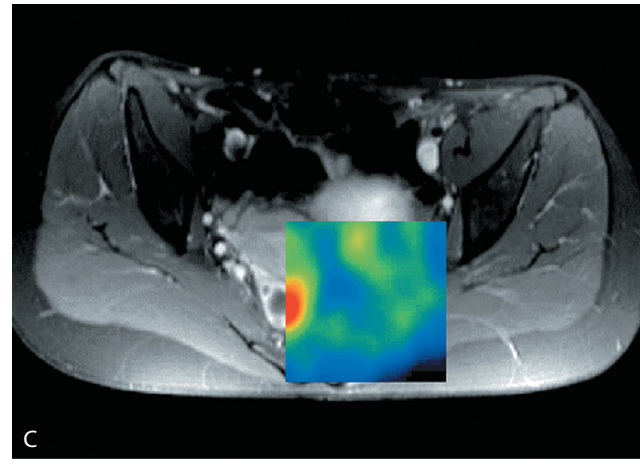

Figure 27.3. Histologically proven nonaffected cystic ovary in a patient with a recurrent yolk sack tumor: T1-weighted, fat-suppressed MR sequence after application of gadolinium–diethylenetriamine pentaacetic acid (Gd-DTPA) (A) depicts a physiologic-appearing cystic ovary (arrow). Corresponding PET (B) revealed a false-positive finding with an increased glucose uptake (arrow) suspect of a recurrent disease. Multimodality display of registered images (C) shows exact spatial correlation between the cystic ovary in MRI and increased glucose uptake in PET.

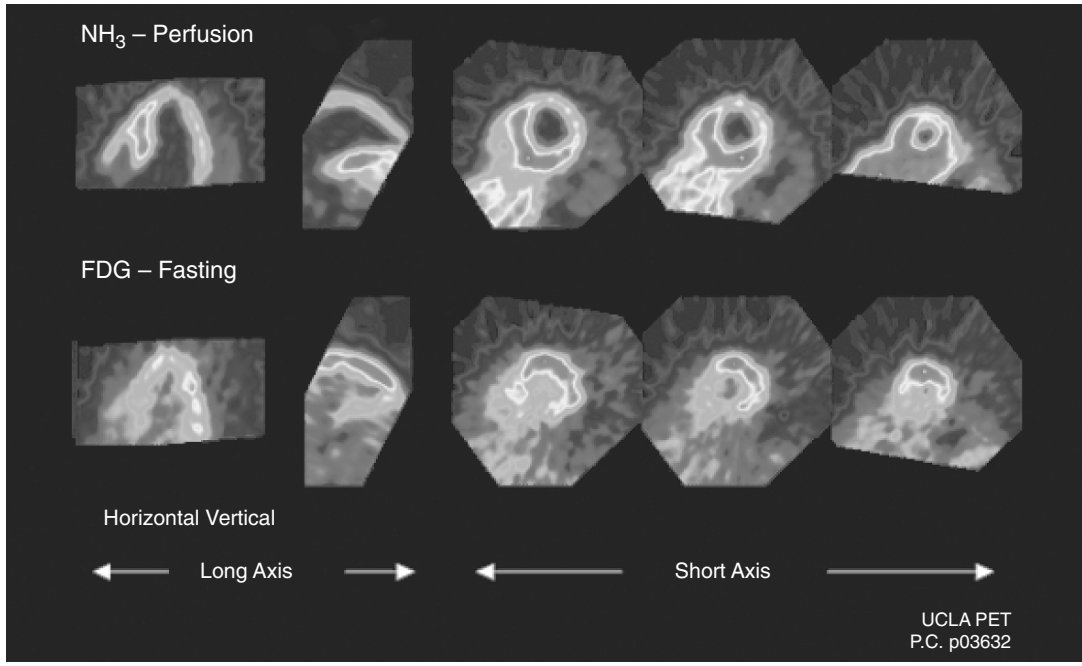

Figure 22.3. Reoriented images of the myocardial ^{13}N-ammonia (upper panel) and fasting ^{18}F-FDG uptake (lower panel) in a patient with transposition of the great arteries who had an acute episode of chest pain late after the arterial switch operation. Note the impaired perfusion in the anterolateral wall evidenced by the decreased uptake of ^{13}N-ammonia, whereas the myocyte metabolism of ^{18}F-FDG is preserved, indicating viable myocardium in that myocardial regions. (Courtesy of Dr. Heinrich Schelbert, David Geffen School of Medicine, Los Angeles.) (See color insert.)

detecting myocardial viability in children with myocardial dysfunction and its correlation with histopathological changes, Hernandez-Pampaloni et al. (45) studied a group of patients with different suspected coronary abnormalities after an acute cardiac event (Fig. 22.3, see color insert). They reported good agreement between the findings on myocardial perfusion PET and metabolic imaging with those on coronary angiography, echocardiography, and histopathology.

Anomalous Origin of the Left Coronary Artery Arising from the Pulmonary Artery

Anomalous origin of the left coronary artery arising from the pulmonary artery (ALCAPA) is a rare but serious congenital anomaly. It does not present prenatally because of the favorable fetal physiology that includes (1) equivalent pressure in the main pulmonary artery and aorta secondary to a nonrestrictive patent ductus arteriosus, and (2) relatively equivalent oxygen concentrations due to parallel circulations. As a result, myocardial perfusion is normal, and there is no stimulus for collateral formation between the right and left coronary artery

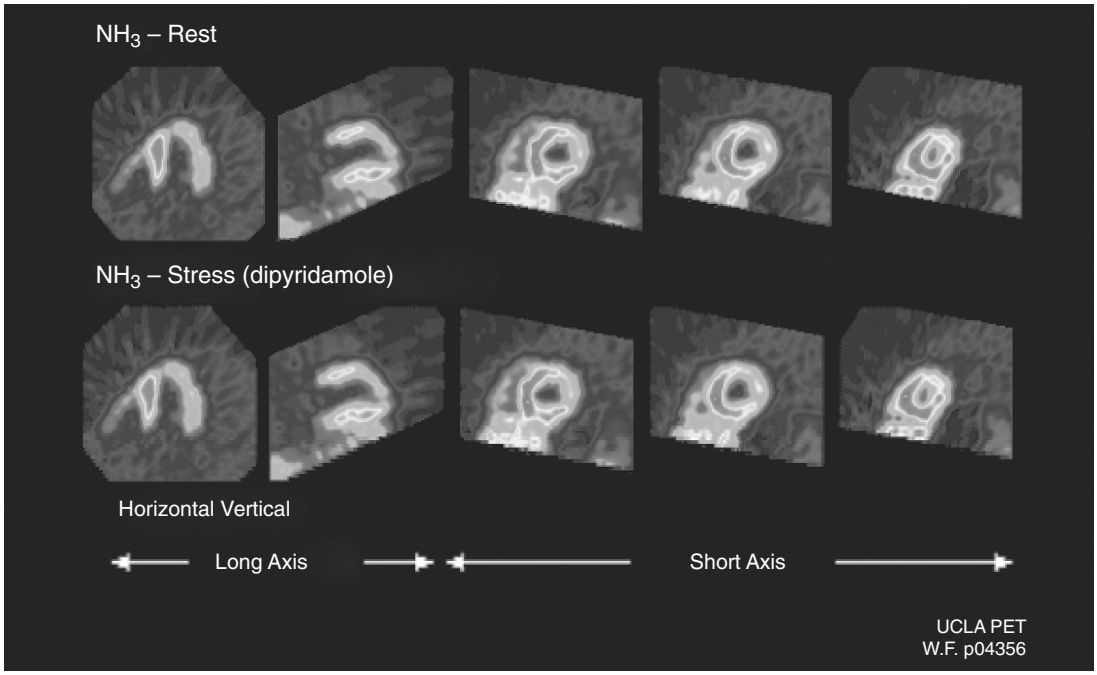

Figure 22.4. Reoriented images of the myocardial resting ^{13}N-ammonia (upper panel) and after dipyridamole-induced stress ^{13}N-ammonia (lower panel) PET study in a patient with anomalous origin of the left coronary artery arising from the pulmonary artery (ALCAPA). Note the fixed defect in the anterolateral wall that corresponds to an acute myocardial infarction in that region. (Courtesy of Dr. Heinrich Schelbert, David Geffen School of Medicine, Los Angeles.) (See color insert.)

systems. In the few weeks after birth, pulmonary artery pressure and resistance progressively decrease with a simultaneous decrease in oxygen content of pulmonary blood flow as the circulation becomes one in series. This results in the left ventricular myocardium being perfused by relatively desaturated blood under low pressure, leading to myocardial ischemia. Initially, myocardial ischemia is transient, occurring during periods of increased myocardial demands, such as when the infant is feeding and crying. Further increases in myocardial oxygen consumption lead to infarction of the anterolateral left ventricular free wall (Fig. 22.4, see color insert). This may lead to possible mitral valve papillary muscle dysfunction and variable degrees of insufficiency. Following surgical repair to establish blood flow to the left coronary arteries from the aorta, left ventricle (LV) function recovers and usually normalizes within 2 to 3 years. Perfusion abnormalities, however, are not uncommon in long-term survivors. Long-term survivors of ALCAPA repair demonstrate regional impairment of myocardial flow reserve. This may contribute to impaired exercise performance by limiting cardiac output reserve (46). Patients with severely reduced regional coronary flow reserve may be at risk of exercise-

induced ischemic events. Thus, accurate identification of these patients by PET imaging can be of help regarding physical activity, antiischemic measures, and revascularization.

Kawasaki Disease

Kawasaki disease, also known as mucocutaneous lymph node syndrome, is an acute vasculitis that mostly affects infants and children under 5 years of age. It causes an acute vasculitis, particularly affecting medium-sized arteries such as the coronary arteries (47). The etiology and pathogenesis of Kawasaki disease remains unknown, although clinical and epidemiologic data support an infectious cause. The clinical features of Kawasaki disease can be divided into three phases. The first, or acute, phase lasts about 10 days and is marked by a temperature as high as 40°C accompanied by a polymorphous exanthem. Cardiac manifestations during this phase may include tachycardia, gallop rhythm, congestive heart failure, pericardial effusion, and arrhythmias. Arthritis and arthralgia occur during the second, or subacute, phase, which is characterized by gradual subsiding of fever, thrombocytosis, and desquamation of the palms and soles. Third is a convalescent phase where children continue to recover and all laboratory studies normalize but aneurysms of the coronary arteries may continue to enlarge (48).

Although this disease appears to be benign and self-limiting in most instances, coronary artery aneurysms or vascular ectasia develop in 20% to 25% of untreated Kawasaki patients and can lead to serious morbidity and even death (48,49). The cardiac lesions in Kawasaki disease occur in different stages, developing from an acute perivasculitis and vasculitis of the microvessels and small arteries to a panvasculitis of the coronary arteries with aneurysms and thrombosis. The late phase of development is characterized by myocardial scarring with severe stenosis in the major coronary arteries (47).

A specific diagnostic test, however, does not exit. Thus, the diagnosis of Kawasaki disease is based on the presence of a fever for at least 5 days as well as the presence at least four of the five classic clinical features: (1) bilateral nonexudative bulbar conjunctival injection, (2) unilateral nonsuppurative cervical adenopathy, (3) oral or lip erythema, (4) edema or erythema of hands and feet, and (5) a polymorphous erythematous rash.

Echocardiography is useful during the acute and subacute phase of the disease for the assessment of ventricular function and to delineate coronary aneurysms or ectasia. Up to 40% of untreated patients with Kawasaki disease have echocardiographically documented coronary artery dilatation and aneurysms in the third or convalescence phase of their disease (50). Cardiac involvement may cause different cardiac events, from silent chest pain to acute myocardial ischemia or sudden death due to myocardial infarction from occlusive coronary artery disease. Incidence, onset, and the time course of stenosis formation in the aneurysm are affected by various factors, such as the diameter of the aneurysm and the location and type of coronary arteries involved.

It is therefore critical to recognize aneurysms in Kawasaki disease to determine effective early therapy and to improve prognosis.

Two-dimensional echocardiography can detect coronary aneurysms. However, this method is not as effective for detecting coronary stenosis. Coronary angiography is an accurate method for assessing large and medium-sized coronary arteries but has little value in detecting microangiopathy (51). Furthermore, angiography is an invasive and potentially harmful procedure, with a nontrivial amount of radiation exposure that cannot be repeated often, especially in the pediatric population. Information about myocardial perfusion and regions of ischemia is necessary to make clinical decisions and to evaluate the prognosis.

In the past, children with a previous history of Kawasaki disease but no detectable angiographic coronary lesions during the acute and subacute phase were thought not to be at risk for myocardial ischemia. More recent studies have demonstrated the presence of reversible myocardial perfusion defects in children with angiographically normal coronary arteries. The clinical significance of these findings remains to be fully addressed (52). An alteration of the coronary microcirculation, possibly the result of a previous inflammatory process, has been suggested as a cause of the abnormalities in myocardial perfusion. Different authors have reported an abnormal hyperemic MBF and an impaired coronary flow reserve in patients with a previous history of Kawasaki disease but normal epicardial coronary arteries, after an adenosine-induced hyperemia PET study (53,54). These microcirculatory abnormalities, which could represent a risk factor for the development of atherosclerosis in adulthood, may correspond to an endothelium-dependent dysfunction. Furuyama et al. (55) described an impaired MBF response to the cold-pressor testing using ^{15}O-H_2O PET in patients with Kawasaki disease, when compared to normal controls, suggesting an intimal hypertrophy in these patients (55). An abnormal endothelium-dependent vasodilation in the brachial artery of patients with a previous history of Kawasaki disease seems to confirm that endothelial dysfunction may at least contribute to the microcirculatory changes responsible for myocardial perfusion alterations.

Positron emission tomography has been used in patients with Kawasaki and demonstrable coronary aneurysms as well to demonstrate an impaired hyperemic and coronary flow reserve, as reported by Ohmochi et al. (56). Interestingly, Yoshibayashi et al. (57) have correlated the presence of ischemic myocardial injury with the appearance of abnormal Q waves in the electrocardiogram (ECG) when compared to a ^{13}N-ammonia and ^{18}F-FDG PET. They reported that the presence of abnormal Q waves is a reliable clue to the presence of ischemic myocardial injury, whereas metabolic PET imaging showed viable myocardial tissue in those areas with an abnormal Q wave (57).

Monitoring the response to different therapies is another area of application of PET imaging. Hwang et al. (58) reported that the incidence of perfusion and metabolic PET abnormalities was reduced in patients in the convalescent stage of Kawasaki disease when they were

treated with a 5-day dose of intravenous (IV) immunoglobulin, compared to those who received only a single dose of IV immunoglobulin.

Coronary arteries that have been previously aneurysmal have an abnormal response to vasodilators in Kawasaki patients. Intravascular ultrasound imaging of the coronary arteries demonstrated increased intimal thickening in many regions of resolved aneurysms but normal intimal thickness in those patients with Kawasaki disease and no previous history of a coronary artery lesion (59). These findings support the continuous surveillance of all children with a history of Kawasaki disease regardless of coronary artery status. Approximately 50% of patients who had coronary aneurysms show regression on follow-up coronary angiography (60). However, these angiographically normal vessels showed intimal thickening and endothelial dysfunction similar to that observed in early atherosclerotic lesions. Because these patients should be followed carefully to monitor potential late effects of Kawasaki disease in the coronary circulation, periodical PET measurement of MBF seems very appropriate in this particular setting. It has been reported that abnormal myocardial perfusion is present long-term after the resolution of complicated Kawasaki disease, and that unfavorable perfusion response to pharmacologic stress was coupled with an abnormal regional contractility. On the other hand, however, enhanced perfusion correlated poorly with segmental contractility response (52). Therefore, even if these abnormalities are modest and do not seem to diminish exercise performance in these patients, these findings may have implications later in life when other coronary risk factors may potentiate the development of coronary artery disease during adulthood.

Cardiac Transplant Vasculopathy

Allograft vasculopathy has emerged as the most important limiting factor for long-term survival and is the leading cause of death 1 year after transplantation. At 10 years after transplantation, as many as 20% of recipients have developed significant allograft vasculopathy. Because the donor heart is denervated, children with graft vasculopathy rarely present with angina. They may have atypical angina such as shoulder or back pain or, more frequently, abdominal pain. They may also present with syncope or sudden death. Several studies have demonstrated the diffuse nature of cardiac allograft vasculopathy, which affects the major epicardial vessels along their entire length from the base of the heart to the apex and the epicardial and intramyocardial branches (61). Available studies suggest that graft vasculopathy has a mixed etiology, based on the varied patterns of vascular disease seen by coronary angiography, that is, either diffuse and circumferential narrowing in the distal parts of the coronary arteries or focal segmental disorder in the middle and proximal branches similar to atherosclerosis. Major histologic findings include intact internal elastic lamina; rarely, calcification; occasionally, a low grade of vasculitis; and a tendency for the disease to progress rapidly (62). Although treatment of transplant vasculopathy is complex, several studies have showed

that focal lesions have been treated successfully with percutaneous transluminal coronary angioplasty (63). On the other hand, the results of coronary artery bypass surgery have not been so successful, leaving only retransplantation as an alternative (64).

Annual coronary angiography and intravascular ultrasound have been used to detect coronary involvement and to assess the development and progression of this disease. These techniques are invasive and not event-free with a potential harmful effect, especially in the pediatric population. Therefore, it is paramount to introduce a noninvasive test to detect the progression of the disease and to predict future long-term outcome and cardiac events. Several studies have demonstrated in the adult population that technetium-based myocardial perfusion studies are useful to screen for significant coronary artery disease in the transplant vasculopathy (65). Additionally, they provide incremental data for the prediction of cardiac death in heart transplant patients, as described by Elhendy et al. (66).

Cardiac PET studies have shown a decreased coronary flow reserve in adult cardiac allografts after pharmacologically stress-induced hyperemia with dipyridamole (67,68). In addition to a decreased exercise capacity, PET imaging has described an incomplete reinnervation in the transplanted adult heart (69).

Cardiomyopathies of Diverse Origin

Cardiac PET has proven to be of utility in monitoring response to therapy and in predicting potential long-term outcome by measuring MBF after corrective surgery in specific cardiomyopathies. Donnelly et al. (70) reported on a small group of patients with a hypoplastic left heart syndrome assessed after corrective surgery, and found that coronary flow reserve was reduced due to a higher resting MBF. Also, long-term survivors of the Mustard operation have shown a high prevalence of right ventricular dysfunction. In these patients a decreased coronary flow reserve, as reported by Singh et al. (71), may help explain the systemic ventricular dysfunction they suffer. The long-term outcome of circulation driven by a single ventricular chamber remains a matter of concern as multiple sequelae, such as thromboembolic complications, ventricular dysfunction, arrhythmias, and reduced exercise capacity, can arise from subtle but continuous circulatory changes (72). Thus, coronary artery blood flow may be compromised if the ventricular mass increases significantly to reduce systolic and diastolic function. Hauser el al. (73) has reported an impaired stress MBF, impaired coronary flow reserve, and an elevated vascular resistance after vasodilation in patients with Fontan-like operations.

In the cardiomyopathy of Duchenne and Becker muscular dystrophies, studies at necropsy have shown that the posterolateral wall of the left ventricle is the first myocardial area suffering from dystrophy even in the absence of small vessel coronary artery disease in these regions. Perloff et al. (74) have reported areas of myocardial hibernation, identified by perfusion and metabolic PET imaging, in the

lateral and posterolateral wall in a group of patients with Duchenne dystrophy.

Very low coronary flow reserve values measured with PET are reported in neonates with surgically treated congenital heart disease (75). Because the chronically dilated extramural coronary arteries in cyanotic congenital heart disease have a limited capacity to dilate further and because myocardial oxygen extraction is inherently maximal, the potential oxygen debt incurred by systemic arterial hypoxemia may be inadequately met. Basal coronary flow as determined by ^{13}N-ammonia PET was increased to the same degree in the right ventricular and left ventricular free walls and in the ventricular septum, but hyperemic perfusion, coronary vascular resistance, and flow reserve were normal in each of the three regions of interest. Although these studies were not designed to determine the mechanism(s) by which flow reserve is preserved in the face of increased basal coronary flow, the results may suggest remodeling of the intramyocardial coronary microcirculation and vasculogenesis in response to hypoxemic stimulation as potential causes for explaining the neonatal myocardial adaptation to different conditions.

Future Directions

Although current cardiac PET clinical applications in pediatrics are still limited, the greater availability of PET systems and infrastructure along with greater knowledge of its capabilities by the pediatric medical community are allowing PET imaging to become more than a tool for the noninvasive assessment of myocardial perfusion and glucose metabolism. It promises to have great potential for applications such as in vivo assessment of cardiac cellular metabolism and receptor function and gene expression. Finally, the potential of combined multimodality imaging, represented by PET–computed tomography (CT) imaging, may provide in the near future real-time assessment of function and structure of the diseased pediatric heart.

References

1. Bax JJ, et al. Metabolic imaging using F18-fluorodeoxyglucose to assess myocardial viability. Int J Card Imaging 1997;13(2):145–155; discussion 157–160.
2. Di Carli MF. Predicting improved function after myocardial revascularization. Curr Opin Cardiol 1998;13(6):415–424.
3. Hubbell JH. Review of photon interaction cross section data in the medical and biological context. Phys Med Biol 1999;44(1):R1–22.
4. Muzik O, et al. Validation of nitrogen-13-ammonia tracer kinetic model for quantification of myocardial blood flow using PET. J Nucl Med 1993; 34(1):83–91.
5. Hutchins GD, et al. Noninvasive quantification of regional blood flow in the human heart using N-13 ammonia and dynamic positron emission tomographic imaging. J Am Coll Cardiol 1990;15(5):1032–1042.

6. Schelbert HR, et al. Regional myocardial perfusion assessed with N-13 labeled ammonia and positron emission computerized axial tomography. Am J Cardiol 1979;43(2):209–218.
7. Bergmann SR, et al. Noninvasive quantitation of myocardial blood flow in human subjects with oxygen-15-labeled water and positron emission tomography. J Am Coll Cardiol 1989;14(3):639–652.
8. Araujo LI, et al. Noninvasive quantification of regional myocardial blood flow in coronary artery disease with oxygen-15-labeled carbon dioxide inhalation and positron emission tomography. Circulation 1991;83(3):875–885.
9. Kaufmann PA, et al. Assessment of the reproducibility of baseline and hyperemic myocardial blood flow measurements with 15O-labeled water and PET. J Nucl Med 1999;40(11):1848–1856.
10. Herrero P, et al. Noninvasive quantification of regional myocardial perfusion with rubidium-82 and positron emission tomography. Exploration of a mathematical model. Circulation 1990;82(4):1377–1386.
11. Tadamura E, et al. Generator-produced copper-62-PTSM as a myocardial PET perfusion tracer compared with nitrogen-13–ammonia. J Nucl Med 1996;37(5):729–735.
12. Beanlands RS, et al. The kinetics of copper-62-PTSM in the normal human heart. J Nucl Med 1992;33(5):684–690.
13. Beller GA, et al. Assessment of regional myocardial perfusion by positron emission tomography after intracoronary administration of gallium-68 labeled albumin microspheres. J Comput Assist Tomogr 1979;3(4):447–452.
14. Melon PG, et al. Myocardial kinetics of potassium-38 in humans and comparison with copper-62–PTSM. J Nucl Med 1994;35(7):1116–1122.
15. Mullani NA, et al. Myocardial perfusion with rubidium-82. I. Measurement of extraction fraction and flow with external detectors. J Nucl Med 1983;24(10):898–906.
16. Choi Y, et al. Quantification of myocardial blood flow using 13N-ammonia and PET: comparison of tracer models. J Nucl Med 1999;40(6):1045–1055.
17. Glatting G, Reske SN. Treatment of radioactive decay in pharmacokinetic modeling: influence on parameter estimation in cardiac 13N-PET. Med Phys 1999;26(4):616–621.
18. Hove JD, et al. Dual spillover problem in the myocardial septum with nitrogen-13–ammonia flow quantitation. J Nucl Med 1998;39(4):591–598.
19. Hutchins GD, Caraher JM, Raylman RR. A region of interest strategy for minimizing resolution distortions in quantitative myocardial PET studies. J Nucl Med 1992;33(6):1243–1250.
20. Hermansen F, et al. Generation of myocardial factor images directly from the dynamic oxygen-15-water scan without use of an oxygen-15-carbon monoxide blood-pool scan. J Nucl Med 1998;39(10):1696–1702.
21. Wyss CA, et al. Bicycle exercise stress in PET for assessment of coronary flow reserve: repeatability and comparison with adenosine stress. J Nucl Med 2003;44(2):146–154.
22. Schelbert HR, et al. Effects of substrate availability on myocardial C-11 palmitate kinetics by positron emission tomography in normal subjects and patients with ventricular dysfunction. Am Heart J 1986;111(6):1055–1064.
23. Brown M, et al. Delineation of myocardial oxygen utilization with carbon-11-labeled acetate. Circulation 1987;76(3):687–696.
24. Brown MA, Myears DW, Bergmann SR. Noninvasive assessment of canine myocardial oxidative metabolism with carbon-11 acetate and positron emission tomography. J Am Coll Cardiol 1988;12(4):1054–1063.

25. Buck A, et al. Effect of carbon-11–acetate recirculation on estimates of myocardial oxygen consumption by PET. J Nucl Med 1991;32(10):1950–1957.
26. Wolpers HG, et al. Assessment of myocardial viability by use of 11C-acetate and positron emission tomography. Threshold criteria of reversible dysfunction. Circulation 1997;95(6):1417–1424.
27. Armbrecht JJ, et al. Regional myocardial oxygen consumption determined noninvasively in humans with (1–11C)acetate and dynamic positron tomography. Circulation 1989;80(4):863–872.
28. Opie LH. Effects of regional ischemia on metabolism of glucose and fatty acids. Relative rates of aerobic and anaerobic energy production during myocardial infarction and comparison with effects of anoxia. Circ Res 1976;38(5 Suppl 1):I52–74.
29. Brosius FC 3rd, et al. Persistent myocardial ischemia increases GLUT1 glucose transporter expression in both ischemic and non-ischemic heart regions. J Mol Cell Cardiol 1997;29(6):1675–1685.
30. Sivitz WI, et al. Pretranslational regulation of two cardiac glucose transporters in rats exposed to hypobaric hypoxia. Am J Physiol 1992;263(3 pt 1): E562–569.
31. Krivokapich J, et al. Fluorodeoxyglucose rate constants, lumped constant, and glucose metabolic rate in rabbit heart. Am J Physiol 1987;252(4 pt 2): H777–787.
32. Laubenbacher C, et al. An automated analysis program for the evaluation of cardiac PET studies: initial results in the detection and localization of coronary artery disease using nitrogen-13–ammonia. J Nucl Med 1993;34(6): 968–978.
33. Tillisch J, et al. Reversibility of cardiac wall-motion abnormalities predicted by positron tomography. N Engl J Med 1986;314(14):884–888.
34. Knuuti MJ, et al. Myocardial viability: fluorine-18-deoxyglucose positron emission tomography in prediction of wall motion recovery after revascularization. Am Heart J 1994;127(4 Pt 1):785–796.
35. Kuhle WG, et al. Quantification of regional myocardial blood flow using 13N-ammonia and reoriented dynamic positron emission tomographic imaging. Circulation 1992;86(3):1004–1017.
36. American Academy of Pediatrics Committee on Drugs: Guidelines for monitoring and management of pediatric patients during and after sedation for diagnostic and therapeutic procedures. Pediatrics 1992;89(6 pt 1): 1110–1115.
37. Practice guidelines for sedation and analgesia by non-anesthesiologists. Anesthesiology 2002;96(4):1004–1017.
38. Tanel RE, et al. Coronary artery abnormalities detected at cardiac catheterization following the arterial switch operation for transposition of the great arteries. Am J Cardiol 1995;76(3):153–157.
39. Wernovsky G, et al. Factors influencing early and late outcome of the arterial switch operation for transposition of the great arteries. J Thorac Cardiovasc Surg 1995;109(2):289–301; discussion 301–302.
40. Weindling SN, et al. Myocardial perfusion, function and exercise tolerance after the arterial switch operation. J Am Coll Cardiol 1994;23(2):424–433.
41. Bengel FM, et al. Myocardial blood flow and coronary flow reserve late after anatomical correction of transposition of the great arteries. J Am Coll Cardiol 1998;32(7):1955–1961.
42. Yates RW, et al. Evaluation of myocardial perfusion using positron emission tomography in infants following a neonatal arterial switch operation. Pediatr Cardiol 2000;21(2):111–118.

43. Hauser M, et al. Myocardial blood flow and flow reserve after coronary reimplantation in patients after arterial switch and Ross operation. Circulation 2001;103(14):1875–1880.
44. Rickers C, et al. Myocardial viability assessed by positron emission tomography in infants and children after the arterial switch operation and suspected infarction. J Am Coll Cardiol 2000;36(5):1676–1683.
45. Hernandez-Pampaloni M, et al. Myocardial perfusion and viability by positron emission tomography in infants and children with coronary abnormalities: correlation with echocardiography, coronary angiography, and histopathology. J Am Coll Cardiol 2003;41(4):618–626.
46. Singh TP, et al. Myocardial flow reserve in long-term survivors of repair of anomalous left coronary artery from pulmonary artery. J Am Coll Cardiol 1998;31(2):437–443.
47. Shulman ST, Rowley AH. Advances in Kawasaki disease. Eur J Pediatr 2004;163(6):285–291.
48. Dajani AS, et al. Diagnosis and therapy of Kawasaki disease in children. Circulation 1993;87(5):1776–1780.
49. Dajani AS, et al. Guidelines for long-term management of patients with Kawasaki disease. Report from the Committee on Rheumatic Fever, Endocarditis, and Kawasaki Disease, Council on Cardiovascular Disease in the Young, American Heart Association. Circulation 1994;89(2):916–922.
50. Kondo C, et al. Detection of coronary artery stenosis in children with Kawasaki disease. Usefulness of pharmacologic stress 201Tl myocardial tomography. Circulation 1989;80(3):615–624.
51. Schillaci O, et al. Technetium-99m sestamibi single-photon emission tomography detects subclinical myocardial perfusion abnormalities in patients with systemic lupus erythematosus. Eur J Nucl Med 1999;26(7):713–717.
52. Iemura M, et al. Long term consequences of regressed coronary aneurysms after Kawasaki disease: vascular wall morphology and function. Heart 2000;83(3):307–311.
53. Muzik O, et al. Quantification of myocardial blood flow and flow reserve in children with a history of Kawasaki disease and normal coronary arteries using positron emission tomography. J Am Coll Cardiol 1996;28(3):757–762.
54. Hauser M, et al. Myocardial blood flow and coronary flow reserve in children with "normal" epicardial coronary arteries after the onset of Kawasaki disease assessed by positron emission tomography. Pediatr Cardiol 2004;25(2):108–112.
55. Furuyama H, et al. Altered myocardial flow reserve and endothelial function late after Kawasaki disease. J Pediatr 2003;142(2):149–154.
56. Ohmochi Y, et al. Assessment of effects of intravenous dipyridamole on regional myocardial perfusion in children with Kawasaki disease without angiographic evidence of coronary stenosis using positron emission tomography and H2(15)O. Coronary Artery Dis 1995;6(7):555–559.
57. Yoshibayashi M, et al. Regional myocardial perfusion and metabolism assessed by positron emission tomography in children with Kawasaki disease and significance of abnormal Q waves and their disappearance. Am J Cardiol 1991;68(17):1638–1645.
58. Hwang B, et al. Positron emission tomography for the assessment of myocardial viability in Kawasaki disease using different therapies. Nucl Med Commun 2000;21(7):631–636.

59. Dahdah NS, et al. Segmental myocardial contractility versus perfusion in Kawasaki disease with coronary arterial aneurysm. Am J Cardiol 1999; 83(1):48–51.
60. Kato H, et al. Long-term consequences of Kawasaki disease. A 10- to 21-year follow-up study of 594 patients. Circulation 1996;94(6):1379–1385.
61. Billingham ME. Histopathology of graft coronary disease. J Heart Lung Transplant 1992;11(3 pt 2):S38–44.
62. Grant SC, Brooks NH, Levy RD. Routine coronary angiography after heart transplantation. Heart 1997;78(2):101–102.
63. Wong PM, et al. Efficacy of coronary stenting in the management of cardiac allograft vasculopathy. Am J Cardiol 1998;82(2):239–241.
64. Halle AA 3rd, et al. Coronary angioplasty, atherectomy and bypass surgery in cardiac transplant recipients. J Am Coll Cardiol 1995;26(1):120–128.
65. Carlsen J, et al. Myocardial perfusion scintigraphy as a screening method for significant coronary artery stenosis in cardiac transplant recipients. J Heart Lung Transplant 2000;19(9):873–878.
66. Elhendy A, et al. Prediction of mortality in heart transplant recipients by stress technetium-99m tetrofosmin myocardial perfusion imaging. Am J Cardiol 2002;89(8):964–968.
67. Zhao XM, et al. Nitrogen-13–ammonia and PET to detect allograft coronary artery disease after heart transplantation: comparison with coronary angiography. J Nucl Med 1995;36(6):982–987.
68. Preumont N, et al. Early alterations of myocardial blood flow reserve in heart transplant recipients with angiographically normal coronary arteries. J Heart Lung Transplant 2000;19(6):538–545.
69. Uberfuhr P, et al. Incomplete sympathic reinnervation of the orthotopically transplanted human heart: observation up to 13 years after heart transplantation. Eur J Cardiothorac Surg 2000;17(2):161–168.
70. Donnelly JP, et al. Resting coronary flow and coronary flow reserve in human infants after repair or palliation of congenital heart defects as measured by positron emission tomography. J Thorac Cardiovasc Surg 1998;115(1):103–110.
71. Singh TP, et al. Myocardial flow reserve in patients with a systemic right ventricle after atrial switch repair. J Am Coll Cardiol 2001;37(8):2120–2125.
72. Fishberger SB, et al. Factors that influence the development of atrial flutter after the Fontan operation. J Thorac Cardiovasc Surg 1997;113(1):80–86.
73. Hauser M, et al. Myocardial perfusion and coronary flow reserve assessed by positron emission tomography in patients after Fontan-like operations. Pediatr Cardiol 2003;24(4):386–392.
74. Perloff JK, Henze E, Schelbert HR. Alterations in regional myocardial metabolism, perfusion, and wall motion in Duchenne muscular dystrophy studied by radionuclide imaging. Circulation 1984;69(1):33–42.
75. Oskarsson G. Coronary flow and flow reserve in children. Acta Paediatr Suppl 2004;93(446):20–25.